CHEMISTRY OF MATERIALS
Cite This: Chem. Mater. 2017, 29, 9162-9170
Article
pubs.acs.org/cm

Unexpected Opposite Influences of Para vs Ortho Backbone Fluorination on the Photovoltaic Performance of a Wide-Bandgap Conjugated Polymer

Mian Cai,[†,‡] Xichang Bao,[†] Yan Fang Liu,[†] Chenchen Li,[†,‡] Xiao Wang,[†] Zhenggang Lan,*[,†] Renqiang Yang,*[,†] and Xiaobo Wan*[,†,‡]

[†]CAS Key Laboratory of Bio-based Materials, Qingdao Institute of Bioenergy & Bioprocess Technology, Chinese Academy of Sciences, 189 Songling Road, Qingdao 266101, People's Republic of China

[‡]University of Chinese Academy of Sciences, Beijing 100049, People's Republic of China

Supporting Information

ABSTRACT: Fluorination density and regioregularity are known factors that have high impact on the performance of organic solar cells; however, due to the limited available fluorination positions, the influence of backbone fluorination positions (such as ortho, para, and meta) has not been well studied. Here we disclose that the fluorination position on a conjugated polymer backbone may have completely opposite effects on its performance. Specifically, compared to the nonfluorinated control, Devices fabricated with the conjugated polymer based on para-fluorinated dibenzo[*c*,*h*][2,6]-naphthyridine-5,11-(6*H*,12*H*)-dione (DBND) block exhibit improved power conversion efficiencies (PCEs) up to 6.55%, while devices fabricated with the conjugated polymer based on ortho-fluorinated DBND block exhibit much worse PCEs as low as 1.44%, although both polymers have similar HOMO/LUMO levels, bandgaps, and backbone torsion angles. It is found that different fluorination positions result in different dipole moments, intermolecular binding energies, and syn/anti conformer ratios, which eventually lead to the distinct phase-separation behaviors of the corresponding solar cells.

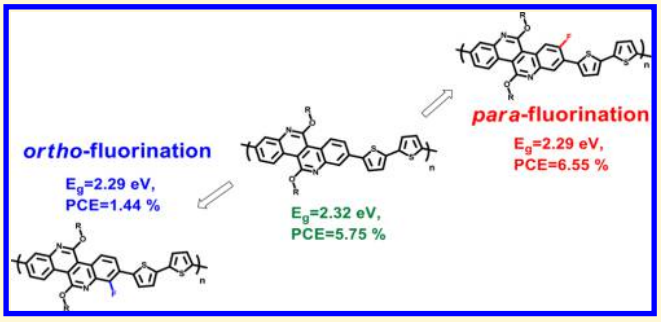

INTRODUCTION

Bulk heterojunction organic solar cells (BHJ-OSCs) have attracted great attention in academic research in the prospect of producing highly efficient, large-area, and high-throughput flexible photovoltaic modules. Most of high-performance donor−acceptor (D−A) type polymeric donors consist of fluorinated acceptor units as building blocks.[1−8]

Fluorine substitution on polymeric backbones has become a unverisal strategy for highly efficient OSCs ever since the first introduction of this method by Yu and co-workers.[9] Fluorination on building blocks such as bithiophene,[10−14] thienothiophene,[15−17] benzothiadiazoles,[18−24] or benzotriazoles[25−27] have been extensively studied and showed improved performance compared to their nonfluorinated analogues. It is generally accepted that fluorination would (1) push down both the highest occupied molecular orbital (HOMO) and lowest unoccupied molecular orbital (LUMO) energy levels of the conjugated polymer simultaneously without an obvious change of the energy gap, which is beneficial to the open-circuit voltage (V_{OC}); (2) induce a larger dipole on the backbone, which results in stronger intermolecular interaction, better exciton dissociation, and longer charge carrier lifetime; (3) promote better planarity of backbone due to the locked-up effect via C−F···S, C−F···H, or C−F···π interactions; and (4) provide better stability of the devices due to the enhanced hydrophobicity.[12,13,28,29]

Despite the well-documented advantages of fluorination outlined above, the influence of fluorination on the properties of the resulting conjugated polymers is actually much more complicated. Sometimes, fluorination does not always result in polymers with improved performance in OSCs. For example, Yu et al. found that fluorination on the benzodithiophenes buliding block in poly(thienothiophene-*co*-benzodithiophenes) led to poor PCE.[15,17] Fluorination density (in many cases, mono- vs difluorination) may also have controversial influences on the OSC performance of the resulting polymers. Shi et al. found that the copolymerization of 3-alkoxy-3′-alkyl-2,2′-bithiophene with difluorinated BT afforded a copolymer with better OSC performance when compared with that obtained from monofluorinated BT.[22,30] On the other hand, Jo et al. found that the polymer based on monofluorinated BT exhibited higher PCE than the one based on difluorinated BT.[19] Osaka and co-workers reported that the polymer based on a heavily fluorinated unit (3,3′4,4′-tetrafluoro-2,2′-bithiophene) ex-

Received: July 18, 2017
Revised: October 13, 2017
Published: October 13, 2017

DOI: 10.1021/acs.chemmater.7b03025
Chem. Mater. 2017, 29, 9162−9170

Scheme 1. Chemical Structures of Fluorinated Polymers

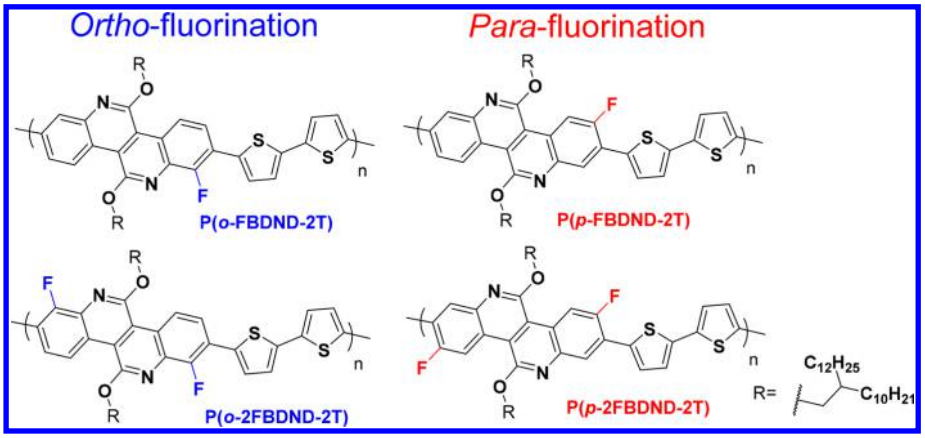

Table 1. Molecular Weights, Optical Properties, and Electrical Properties of Fluorinated DBND-Based Polymers

polymer	M_n[a] (kDa)	PDI[a]	λ_{max}[b] (nm)	λ_{edge}[b] (nm)	E_g^{opt} (eV)	IP[c] (eV)
P(*o*-FDBND-2T)	63.6	2.71	476, 511	541	2.29	5.68
P(*o*-2FDBND-2T)	57.3	2.29	476, 513	539	2.29	5.65
P(*p*-FDBND-2T)	136.0	3.34	481, 515	542	2.29	5.65
P(*p*-FDBND-2T)[d]	75.8	3.32	480, 515	541	2.29	5.65
P(*p*-2FDBND-2T)	67.1	2.39	488, 522	547	2.27	5.72

[a]Determined by GPC at 150 °C using TCB as the eluent. [b]Films are prepared by spin-coated the polymer solution on the piezoid. [c]Films are prepared by drop-casting the polymer solution on the working electrode. [d]P(*p*-FDBND-2T) with lower molecular weight was prepared by shortening the reaction time.

hibited worse PCE compared with the one based on the lightly fluorinated unit (3,3′-difluoro-2,2′-bithiophene).[13] Changing the incorporation ratio of the fluorinated units vs non-fluorinated units in the polymeric chain may improve the PCE,[16,26] due to the change of HOMO/LUMO energy levels or the improved hole mobility. The regioregularity of the fluorinated units in the polymer is also an important factor.[28,31] It was found that the regioregular polymer had a higher dipole moment, which preferred stronger interchain packing mode.[28] All these results suggest that although fluorination is a powerful way to improve the performance of OSCs, the effects of the fluorination need to be carefully evaluated.

Besides these factors, another factor that might influence the OSC performance is the location of fluorinations (ortho, para, or meta) on the polymeric backbone. However, little was known about this factor, presumably due to the availability of such a fluorinated monomer. Most of fluorinated monomers mentioned above could not provide adjustable fluorination locations, but only the selection for either mono- or difluorination. We noticed that several reports on the influence of the fluorination locations on the side chains have been reported.[32−34] For example, Cho et al. reported that ortho- and meta-fluorination on the side chain of a two-dimentional conjugated polymer have different effects on OSC performance. They found that although ortho-fluorination led to a lower LUMO level, it also forced the backbone to adopt a more twisted conformation due to the imposed steric hindrance, which led to a worse PCE.[34] Intriguingly, in the study of organic field-effect transistors, Pei and co-workers found that the polymer with backbone fluorination at the ortho-position showed a 2-fold enhancement of charge carrier mobility compared with the one with fluorination at the para-position.[35] This result infers that the control of backbone fluorination positions might also have a drastic influence also on OPVs, which deserves further study.

Here we report an example showing that changing the fluorination locations on the conjugated polymeric backbone may have a drastic influence on OSC performance. The effects of para- and ortho-fluorination on the acceptor unit of a wide-bandgap conjugated polymer based on dibenzo[*c*,*h*][2,6]-naphthyridine-5,11-(6*H*,12*H*)-dione (DBND)[36] were thoroughly investigated. Compared with the nonfluorinated control that exhibited a PCE of 5.75%, para-fluorinated and ortho-fluorinated (to the N atom) DBND (denoted as *p*-FDBND and *o*-FDBND, respectively) have completely opposite effects on the OSC performance of the resulting polymers: *p*-FDBND gave a polymer with an improved PCE up to 6.55%, which is the highest among the polymer donors with a bandgap around 2.30 eV, while *o*-FDBND resulted in a polymer with a much worse PCE (1.44%). We showed that in this case the location of fluorination is the key factor for such opposite effects, overwhelming other factors such as fluorination density and regioregularity. The reasons for such a drastic different performance were studied in detail both theoretically and experimentally. It was revealed that the different fluorinated positions greatly influenced the polarity and aggregation behavior of the resulting polymers, hence the nanoscale phase separation in the bulk heterojunctions, which was not observed before.

RESULTS AND DISCUSSION

General Characterization of the Fluorinated Polymers. Specifically, to investigate the influence of the fluorination position on the OSC performance of DBND-based polymers, four fluorinated DBND-based polymers were synthesized according to the method developed in our group[36] (for details, see the Supporting Information). Mono- and di-

DOI: 10.1021/acs.chemmater.7b03025
Chem. Mater. 2017, 29, 9162−9170

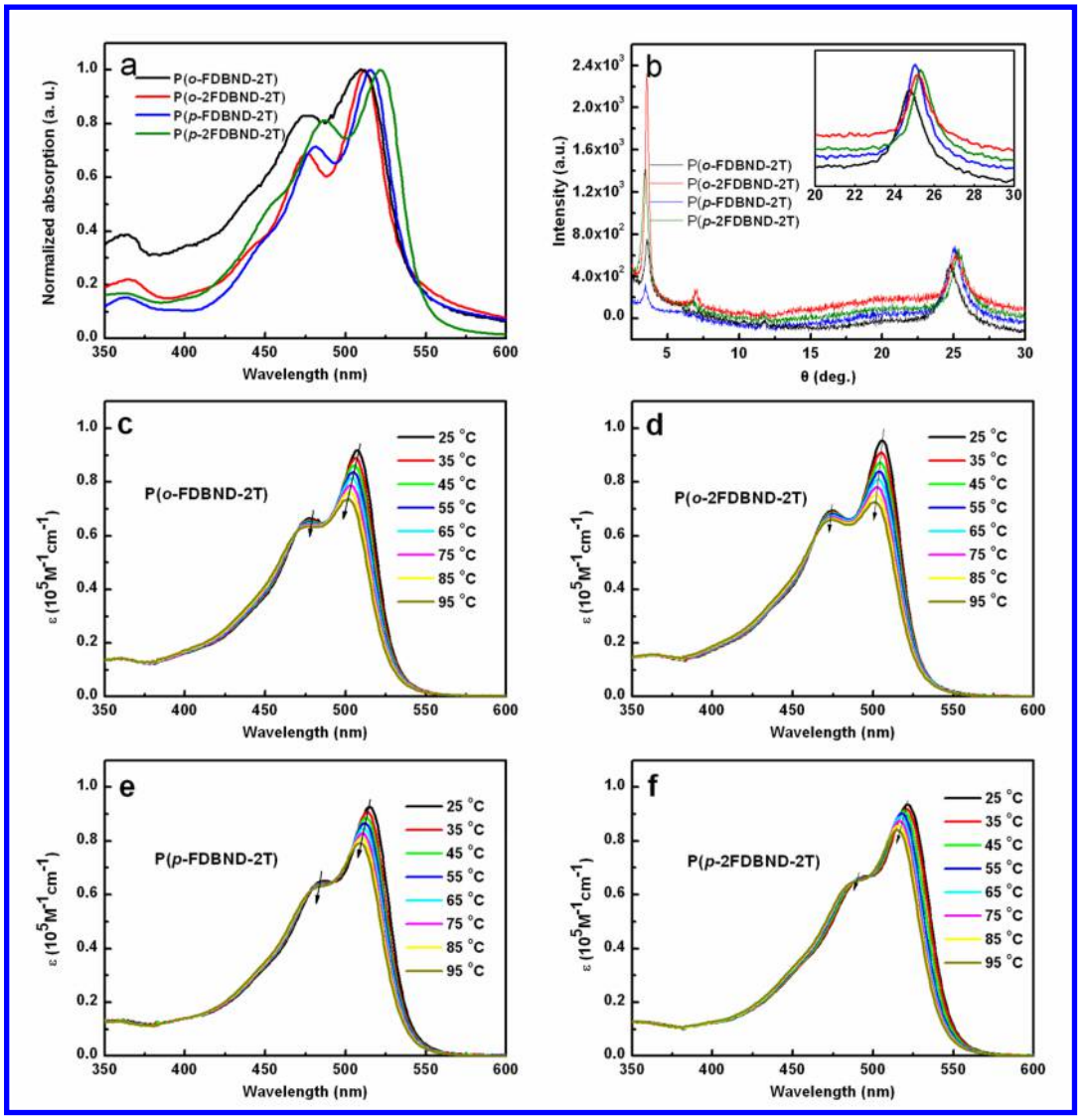

Figure 1. (a) UV/vis absorption spectra of fluorinated polymer films. (b) Out of plane XRD pattern of neat polymer films. (c–f) Temperature-dependent UV–vis absorption spectra of P(*o*-FDBND-2T), P(*o*-2FDBND-2T), P(*p*-FDBND-2T), and P(*p*-2FDBND-2T) in diluted *o*-DCB (0.01 g L^{-1}).

ortho-fluorinated polymers are denoted as P(*o*-FDBND-2T), P(*o*-2FDBND-2T), while mono- and di-para-fluorinated polymers are denoted as P(*p*-2FDBND-2T) and P(*p*-FDBND-2T), respectively, as shown in Scheme 1. In monofluorinated polymers, the fluorinated units were incorporated regio-irregularly. The molecular weights of the polymers were determined via gel permeation chromatography (GPC) using 1,2,4-trichlorobenzene as the eluent at 150 °C after calibration against polystyrene standards. The average molecular weights (M_n) and polydispersity index (PDI) are shown in Table 1. P(*o*-FDBND-2T), P(*o*-2FDBND-2T), and P(*p*-2FDBND-2T) show similar M_n in the range of 57–67 kDa, while P(*p*-FDBND-2T) obtained under the same polymerization conditions exhibits a high M_n up to 136 kDa. For comparison, we also synthesized P(*p*-FDBND-2T) with lower Mn (75.8 kDa) by shortening the polymerization time.

Very interestingly, para-fluorinated polymers and ortho-fluorinated polymers show very different solubilities and aggregation behaviors in solution. Both ortho-fluorinated polymers exhibit an excellent solubility in *o*-dichlorobenzene (*o*-DCB) up to 15 mg mL^{-1} at 100 °C, while both para-fluorinated polymers show much lower solubility in *o*-DCB around 6 mg mL^{-1} at 100 °C. Moreover, upon cooling to room temperature, the solution of P(*p*-2FDBND-2T) formed organogels, and the solution of P(*p*-FDBND-2T) became very viscous, which is not observed for ortho-fluorinated polymers.

Such different aggregation behaviors were monitored via temperature-dependent UV–vis absorption spectroscopy in dilute *o*-DCB solutions with temperature ranging from 25 to 95 °C, and the results are shown in Figure 1c–f. Different from many other fluorinated conjugated polymers, the intermolecular charge-transfer (ICT) absorption peak of which vanishes at high temperature,[28] all the fluorinated polymers show a remarkable stability of the ICT absorption even when the temperature was raised to 95 °C, indicating that a strong intermolecular stacking still exists at high temperature, which might be attributed to the contribution of the highly planar DBND structure. However, the aggregation stability of para- and ortho-fluorinated polymers is different. Regardless whether it is mono- or difluorination, the ICT absorption peak (the peak around 510 nm) of both ortho-fluorinated polymers

DOI: 10.1021/acs.chemmater.7b03025
Chem. Mater. 2017, 29, 9162–9170

Table 2. Calculated Character of *o*-2FDBD-2T and *p*-2FDBD-2T

	o-2FDBD-2T		*p*-2FDBD-2T	
	syn-type	anti-type	syn-type	anti-type
μ_g[a] (D)	0.4838	0.4809	0.4864	0.5335
relative free energy[b] (kcal mol^{-1})	0.61	0	1.63	0
relative population[c] (%)	26	74	6	94

[a]The dipole moments (μ_g) of the ground states were calculated by high-level correlated methods ADC(2) using the Turbomole 6.5 program. [b]The final free energies include thermal correction and dispersion correction at ωB97XD/6-31G* level using the Gaussian 09 program. [c]Relative populations of syn/anti conformer were approximated using the Boltzmann equation at 298 K.

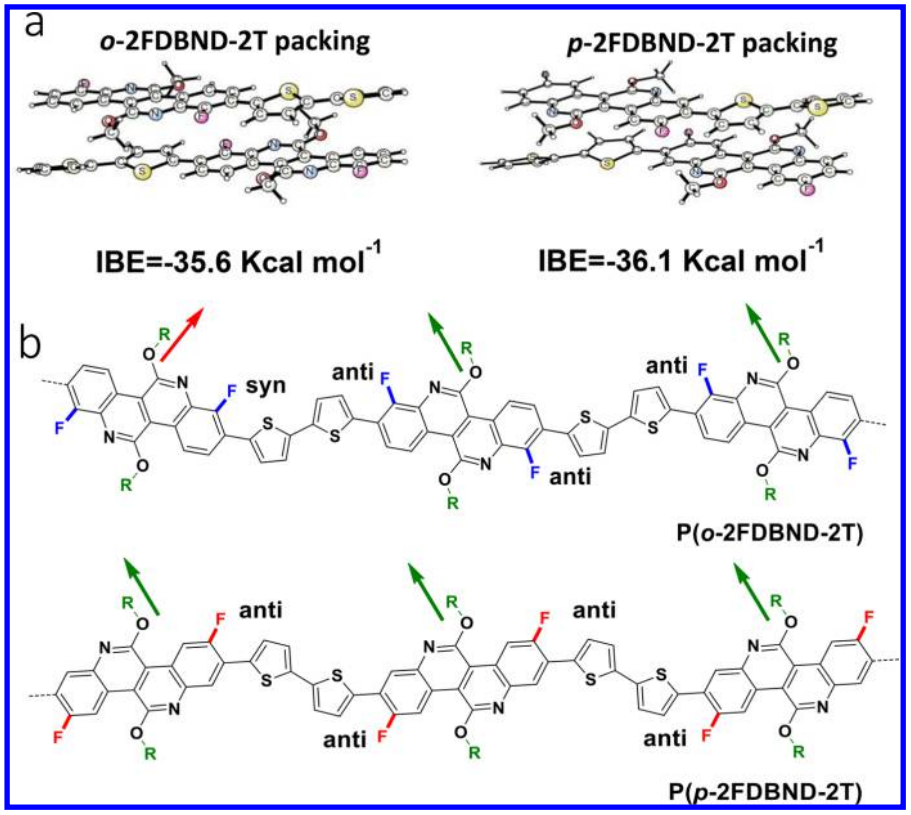

Figure 2. (a) Converged intermolecular packing and the binding energy (IBE) of *o*-2FDBND-2T and *p*-2FDBND-2T in anti-conformation. (b) Proposed syn-anti-anti-anti conformer of *o*-2FDBND-2T (containing 25% syn conformation) and all-anti conformer of *p*-2FDBND-2T with different alkyl orientation.

shows a more obvious decay than that of para-fluorinated polymers with the increase of the temperature, indicating that even stronger interchain interactions exist in para-fluorinated polymers.

The UV−vis absorption spectra of polymers films before and after annealing are presented in Supporting Information Figure S2. As can be seen from Figure S2, the annealing process has different effects on ortho-fluorinated polymers. For both para-fluorinated polymers, there is an increase of the intensity of the ICT peaks (relative to its shoulder peak), and P(*p*-2FDBND-2T) even exhibits a red shift about 10 nm after annealing. For both ortho-fluorinated polymers, there is no obvious change of the absorption peak before and after annealing. It seems there is further crystal growth of para-fluorinated polymers during the annealing process, while such growth does not exist in ortho-fluorinated polymers. This result is in accordance with the different solubility of the two polymers: ortho-fluorinated polymers exhibit better solubility, which allows the formation of well-defined crystals during the slow solvent evaporation process and thus no further growth of crystals is observed during annealing; on the other hand, para-fluorinated polymers show poorer solubility, which leads to the fast formation of a vast amount of nuclei centers and leaves little time for these nuclei to grow due to a fast precipitation process; therefore annealing would help the further growth of polymer crystal.

Theoretical Calculations. To explain the different aggregation behaviors of para- and ortho-fluorinated polymers, we calculated the intermolecular binding energies (IBE) of both ortho- and para-difluorinated repeating units (*o*-2FDBND-2T and *p*-2FDBND-2T) as the simplified model, using density functional theory (DFT) calculation with ωB97XD method, and the long alkyl chains were replaced by methyl groups for simplicity.[29,37] Given that competition between F···S interaction and F···H interaction might exist, the preference of the dimer toward either syn (F and S atoms located on the same side) or anti (F and S atoms located on the opposite sides) conformation is considered first. The torsion profiles, dipole moments and relative free energy as well as anti/syn relative population of *o*--2FDBND-2T and *p*-2FDBND-2T in vacuum are illustrated in Figure S3 and Table 2, respectively. For both

DOI: 10.1021/acs.chemmater.7b03025
Chem. Mater. 2017, 29, 9162−9170

Table 3. Average Performance Parameters of Optimal Solar Cells

polymer	film thickness (nm)	μ_h (cm^2 v^{-1} s^{-1})	V_{OC} (V)	J_{SC} (mA cm^{-2})	FF	PCE[a] (%)
P(*o*-FDBND-2T)	232 ± 35	3.10×10^{-5}	0.87 ± 0.01	2.63 ± 0.09	0.62 ± 0.00	1.44 (1.39 ± 0.05)
P(*o*-2FDBND-2T)	265 ± 12	5.35×10^{-5}	0.89 ± 0.02	1.50 ± 0.07	0.56 ± 0.02	0.79 (0.74 ± 0.05)
P(*p*-FDBND-2T)	280 ± 40	2.35×10^{-4}	0.89 ± 0.02	10.12 ± 0.89	0.66 ± 0.06	6.55 (6.16 ± 0.39)
P(*p*-2FDBND-2T)	220 ± 25	1.42×10^{-4}	0.90 ± 0.02	7.86 ± 1.07	0.67 ± 0.06	5.27 (4.85 ± 0.42)

[a]Optimal polymer:$PC_{71}BM$ ratio is 1:2.

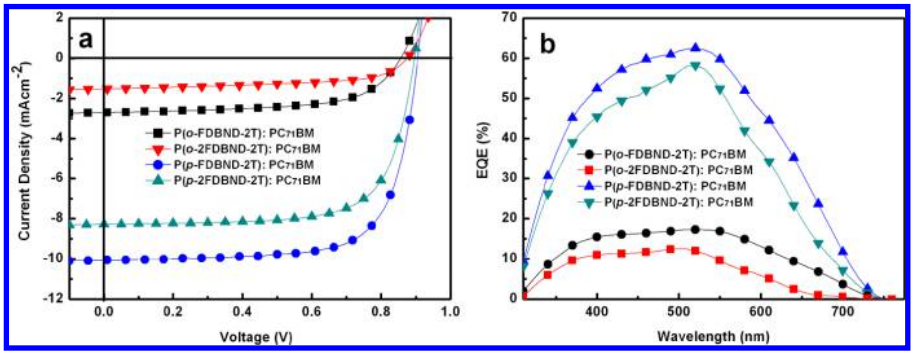

Figure 3. Photovoltaic characteristics: *J*–*V* curves (a) and EQE plots (b) of optimal solar cells under the illumination of AM 1.5G 100 mW cm^{-2}.

repeating units, anti conformation is dominating, showing that F···H interaction is preferred. However, the relative populations are different. The anti/syn ratio is 94/6 for *p*-2FDBND-2T, inferring that the polymer adopts a conformation closer to an all-anti structure, which might enhance the crystallizing capability. On the other hand, the anti/syn ratio in *o*-2FDBND-2T is lower (74/26), indicating that the percentage of syn conformation in the ortho-fluorinated polymer increases compared to para-fluorinated polymer, which might lead to a more curvy backbone and more alkyl side chains not pointing to the same direction (Figure 2b). The calculated dipole moments and IBEs of *o*-2FDBND-2T and *p*-2FDBND-2T are listed in Table 2. Specifically, in the thermodynamically most stable anti conformation, the dipole moment of *p*-2FDBND-2T (0.5335D) is higher than that of *o*-2FDBND-2T (0.4809D), and the IBE of *p*-2FDBND-2T is −36.1 kcal mol^{-1}, higher than that of *o*-2FDBND-2T (−35.6 kcal mol^{-1}). The stronger binding energy of para-fluorinated repeating unit might result from its larger dipole moments,[28] which leads to stronger interchain aggregation.[37,38]

The crystallinity of the fluorinated polymers is illustrated in the out of plane X-ray diffraction (XRD) patterns of the neat films in Figure 1b. All four polymers exhibit obvious lamellar stacking peaks; however, the finer reflection peaks of difluorinated polymers P(*o*-2FDBND-2T) and P(*p*-2FDBND-2T) indicate that the increase of fluorination density promotes better polymer packing. Ortho-fluorinated polymers exhibit stronger 100 lamellar stacking peaks than the para-fluorinated polymers, indicating that the neat films of ortho-fluorinated polymers exhibit higher crystallnity, which is consistent with the UV–vis results of the annealed films. Since an ideal "face on" alignment would give an orthorhombic signal in the XRD pattern, the clearly observed lamellar stacking peaks and π–π stacking peaks indicate multiple orientation in the bulk films. More importantly, the π–π distances calculated for P(*o*-FDBND-2T), P(*o*-2FDBND-2T), P(*p*-FDBND-2T), and P(*p*-2FDBND-2T) are 3.57, 3.50, 3.53, and 3.48 Å, respectively, suggesting that para-fluorinated polymers in solid state show smaller π–π distance compared to ortho-fluorinated polymers, which is consistent with the results of DFT calculation.

Energy Levels and Photovoltaic Properties. The HOMO/LUMO energy levels and the energy gaps (E_g) of the four fluorinated polymers were determined by UV–vis spectra and cyclic voltammetry diagrams of the corresponding thin films (Figure 1a and Figure S4), and the data are shown in Table 1. The fluorinated polymers exhibit similar optical bandgaps (E_g^{opt}) ranging from 2.27 to 2.29 eV, slightly smaller than the corresponding nonfluorinated counterpart (2.32 eV).

The ionization potentials (IP, an estimation of HOMO energy level) of the fluorinated polymers are ranging from 5.65 to 5.72 eV, obviously lower than that of the nonfluorinated counterpart (5.51 eV), showing that fluorination has more profound influence on HOMO energy levels over E_g^{opt}. It should be point out that the UV–vis spectra and IP of P(*p*-FDBND-2T) polymer with realtively lower M_n show barely no difference than that with higher M_n, suggesting that polymer with a M_n of 75.8 kDa may exhibit a performance similar to the one with a M_n of 136 kDa.

Surprisingly, despite their similar HOMO/LUMO energy levels and E_g^{opt}, ortho- and para-fluorinated polymers exhibit distinctly different performance in solution-processed bulk heterojunction devices (device structure: ITO/V_2O_5 (O_2 plasma treated)/polymer:$PC_{71}BM$/Ca/Al), as shown in Table 3 and Figure 3a. Compared with the nonfluorinated counterpart which exhibited a PCE of 5.75%,[36] ortho-fluorinated polymers exhibit rather low PCEs (1.44% for monofluorinated P(*o*-FDBND-2T) and 0.74% for difluorinated P(*o*-2FDBND-2T), respectively), showing that ortho-fluorination has a negative effect on the OPV performance. The addition of DIO shows little improvement on the performance of the devices. On the contrary, para-fluorinated polymers exhibit comparable or even better performance than that of the nonfluorinated counterpart: P(*p*-2FDBND-2T)-based OSCs exhibit a high PCE of 5.27% in the optimized conditions with the open-circuit voltages (V_{OC}) of 0.90 V, short-circuit current (J_{SC}) of 7.86 mA cm^{-2}, and FF of 0.67, and P(*p*-FDBND-2T)-based OSCs exhibit an outstanding performance with V_{OC} of 0.89 V, J_{SC} of 10.12 mA cm^{-2}, FF of 0.66, and PCE of 6.55%. We noticed that P(*o*-FDBND-2T), P(*o*-2FDBND-2T), and P(*p*-2FDBND-2T) have comparable M_n, while P(*p*-FDBND-

DOI: 10.1021/acs.chemmater.7b03025
Chem. Mater. 2017, 29, 9162–9170

2T) shows much higher M_n. To rule out the influence of M_n on PCE, we also synthesized P(*p*-FDBND-2T) with relatively lower M_n (75.8 kDa, comparable to the other three polymers) and characterized its photovoltaic properties. The performance of P(*p*-FDBND-2T) with lower M_n also exhibits a high PCE of 6.21%, with V_{OC} of 0.89 V, J_{SC} of 10.38 mA cm^{-2}, and FF of 0.66 (Figure S5). Thus, when the molecular weight increases from 75.8 to 136 kDa, the increase of PCE is only around 0.34%, which is consistent with their similar UV−vis absorption and ionization potentials and confirms that the molecular weight is not the major reason accounting for the drastic different performances of para- and ortho-fluoroinated polymers. Futhermore, for both ortho- and para-fluorinated polymers, the devices based on monofluorinated polymer show slightly better performance than the difluorinated counterpart, showing that lower fluorination density has a marginal positive effect on PCEs; however, it does not challenge the decisive influence of fluorination locations in this case.

The completely opposite effects of para vs ortho backbone fluorinations on the OPV performance of the corresponding polymers are unexpected. As discussed before, fluorination on the backbone generally has positive effects on the OPV performance compared to those nonfluorinated ones. In our case, ortho-fluorination of the polymer backbone leads to adverse effects on the OPV performance, but mono- and para-fluorination of the polymer backbone lead to an improvement on the OPV performance. It has been reported that when fluorination occurs on the side chain, the different fluorination positions may induce different torsion angles of the backbone, and larger torsion angle leads to poorer performance.[34] However, the torsion angles between the adjacent units for both para- and ortho-fluorinated DBND-based polymers in the optimized conformation are close to 25° according to the DFT calculation, so the influence of fluorination positions on the torsion angle of the backbone could be ruled out. Noticeably, V_{OC} of the devices of four polymers are very similar (ranging from 0.87 to 0.90 V), and the drastic difference of PCE is originated from the remarkable difference in J_{SC} (2.63 for P(*o*-FDBND-2T) vs 10.12 mA cm^{-2} for P(*p*-FDBND-2T), respectively), which is in accordance with their external quantum efficiency (EQE) and the SCLC results (SI, Figure S5): blended films obtained from para-fluorinated polymers show a hole mobility one order higher than ortho-fluorinated ones.

Current−light intensity dependence measurements are used to evaluate the bimolecular recombination process in these polymers, and the results are shown in Figure 4. The relationship between J_{SC} and light intensity (P) can be described by the formula of $\log(J_{SC}) \propto S \log(P)$. If all free charge carriers are swept out and collected at the electrodes prior to recombination, S should be equal to 1, while $S < 1$ indicates the existence of bimolecular recombination. As is seen from Figure 4, the slopes S are calculated as 0.999, 0.993, 0.976, and 0.982 for P(*p*-FDBND-2T), P(*p*-2FDBND-2T), P(*o*-FDBND-2T), and P(*o*-2FDBND-2T), respectively, indicating that P(*p*-2FDBND-2T)- and P(*p*-FDBND-2T)-based OSCs exhibit limited bimolecular recombination but the bimolecular recombination that exists in P(*o*-FDBND-2T) and P(*o*-2FDBND-2T) active layers is a little bit more severe. Such a small difference should not be decisive for the drastically different performance. There are other reasons accounting for the drastic differences in the OPV performances for ortho- and para-fluorinated polymers.

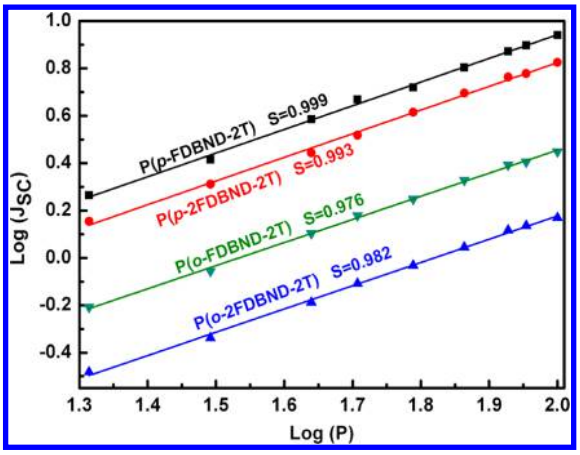

Figure 4. Current−light intensity dependence measurements of four polymers. Light intensity ranges from 20 to 100 mW cm^{-2}.

Morphology Characterization. The poorer performance of devices based on ortho-fluorinated polymers suggests that they may have distinct morphologies from para-fluorinated polymers, as evidenced by transmission electron microscopy (TEM), shown in Figure 5. For both mono- and di- ortho-fluorinated polymers, their blended films with $PC_{71}BM$ contain large polymer domains up to 200 nm in width (Figure 5a,b), indicating the formation of overaggregated polymer domains which is far beyond the typical exciton diffusion lengths for conjugated polymers (~20 nm).[39,40] On the other hand, for both mono- and di- para-fluorinated polymers, their blended films with $PC_{71}BM$ exhibit much smaller polymer domains with less than 20 nm in width and form well-developed nanowire-like fibril networks (Figure 5c,d), which is in the range of the typical exciton diffusion lengths for conjugated polymers. We could also conclude from these images that compared with

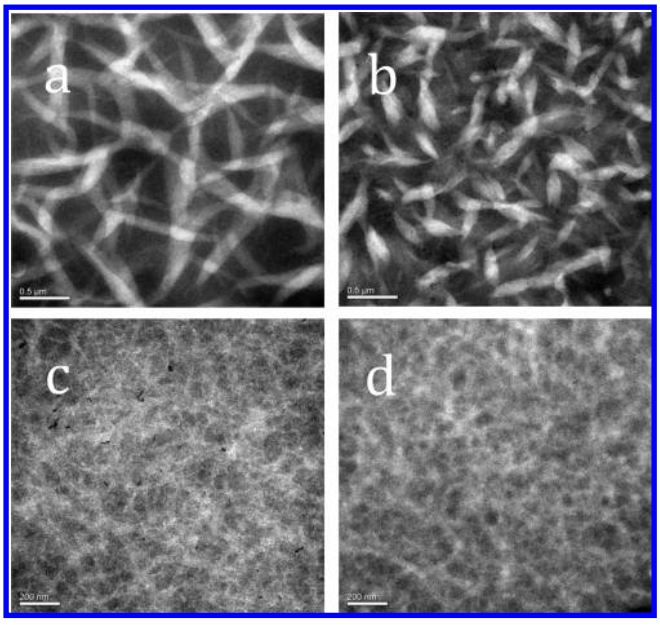

Figure 5. TEM images of the active layers containing (a) P(*o*-FDBND-2T), (b) P(*o*-2FDBND-2T), (c) P(*p*-FDBND-2T), and (d) P(*p*-2FDBND-2T) blended with $PC_{71}BM$ (1:2 (w/w)).

DOI: 10.1021/acs.chemmater.7b03025
Chem. Mater. 2017, 29, 9162−9170

fluorination density (mono- vs difluorination), fluorination positions (ortho vs para) are the major factors controlling the morphology of the blended films. This evidence explicitly indicates that the poorly nanoseparated phase in ortho-fluorinated polymers based devices causes more exciton recombination and results in low J_{SC} and PCE. On the contrary, para-fluorinated polymers based devices exhibit well-separated nanostructures which favors exciton separation and results in much higher J_{SC} and PCE.[41]

We postulate that the differences of ortho- and para-fluorinated polymers in phase separation are directly related to their aggregation ability and solubility. As discussed before, ortho- and para-fluorination result in different dipole moments, IBEs, and syn/anti ratios of the corresponding polymers. Ortho-fluorinated polymers exhibit smaller dipole moments and IBEs, and less well-oriented side chains due to the higher percentage of syn conformer, which means that the interchain interaction of ortho-fluorinated polymers is weaker, leading to their better solubility and more temperature-dependent aggregation behavior in solution state. The better solubility and weaker interaction increase the time needed for aggregation[42] and reduce the number of crystal seeds at the beginning of film fabrication,[43,44] which eventually lead to the formation of larger polymeric domains. On the contrary, para-fluorinated polymers exhibit larger dipole moments and IBEs, and more well-oriented side chains due to the nearly all-anti conformer, which means that the interchain interaction of para-fluorinated polymers is stronger and leads to their poorer solubility and less temperature-dependent aggregation behavior. Thus, once the temperature is cooling, a larger amount of crystalline nuclei are formed due to the pre-existing aggregated polymer chains even at elevated temperature, and quickly precipitate out from the solution to form nanofibrils with much smaller diameter.[43,44]

CONCLUSIONS

In summary, DBND-based conjugated polymers gave us an opportunity to investigate, for the first time, the effects of para- and ortho-fluorination of polymer backbone on the OPV performance of the corresponding polymers. Unexpectedly, completely opposite effects of ortho- and para-fluorination were observed, although all fluorinated polymers show very similar bandgaps, HOMO/LUMO energy levels, and backbone torsion angles. Theoretical calculations point out that different fluorination positions lead to different dipole moments, IBEs, and syn/anti ratios of the resulting polymers, which eventually leads to the different aggregation behaviors in BHJ devices. Ortho-fluorinated DBND polymers exhibit weaker intermolecular interactions and lead to better solubility and the formation of larger polymeric domains, which is detrimental to exciton separation. On the other hand, para-fluorinated DBND polymers exhibit stronger intermolecular interactions, which lead to poorer solubility and the formation of much smaller well-developed nanowire-like fibrils networks, which is beneficial to exciton separation. As a consequence, P(*p*-FDBND-2T)-based OSCs exhibit a PCE of 6.55%, 4.5 times better than P(*o*-FDBND-2T), which also makes P(*p*-FDBND-2T) the first polymer with an E_g close to 2.30 eV but still possessing a PCE over 6%, which efficiently utilizes the energy-rich part (450−550 nm) of the visible sun light. These results suggest that the control of fluorination positions on the polymeric backbone may have a profound influence on the outcome of the OSC performance, which should be paid attention to for the design of conjugated polymers for better OSC devices.

EXPERIMENTAL SECTION

General Procedures. All glassware was completely dried before use. Reagents and solvents were purchased from commercial suppliers or purified by standard techniques. Reactions were monitored by thin-layer chromatography by exposure to UV light irradiation at 254 and 365 nm and/or immersion in a phosphomolybdic acid staining solution followed by drying. Column chromatography was carried out by using silica gel of 200−300 mesh. ^{1}H NMR and ^{13}C NMR spectra were attained from a Bruker AVANCE-III 600 MHz with tetramethylsilane (TMS) as an internal standard at 298 K and $CDCl_3$ or DMSO-d_6 was used as the solvent. The coupling constants J are given in hertz. Cyclic voltammetry (CV) curves were measured by drop-casting polymer film on the working electrode. The measurements were performed on an electrochemistry workstation (CHI660D, Chenhua Shanghai) in anhydrous argon saturated acetonitrile solution (10^{-3} mol L^{-1}) of 0.1 M tetrabutylammonium hexafluorophosphate (n-Bu_4NPF_6) at room temperature by a three-electrode system, which utilizes glassy carbon electrode as the working electrode, Pt as the counter electrode, and a Hg/Hg_2Cl_2 as the reference electrode at a potential scan rate of 0.1 V s^{-1}. The potential of the reference electrode in acetonitrile was identified by using ferrocene as internal standard. The UV−vis spectra were collected with a Hitachi U-4100 UV−vis spectrophotometer in an anhydrous *o*-dichlorobenzene solution (2.5×10^{-5} mol L^{-1}) or on a piezoid spin-coated with polymer solution. Gel permeation chromatography (GPC) was performed with a Waters 1151 pump and UV−vis monitor (700 nm) using 1,2,4-tricholorobenzene (TCB) as eluent (150 °C). Bright-field transmission electron microscopy (TEM) data were acquired using a HITACHI H-7650 electron microscope. Grazing incidence wide-angle X-ray scattering (GIWAXS) measurements were performed at beamline BL16B1 of the Shanghai Synchrotron Radiation Facility (SSRF). Samples were prepared on Si substrates using the same preparation conditions as for devices. The 10 keV X-ray beam was incident at a grazing angle of 0.2. XRD patterns were investigated with a Rigaku D/MAX-2500 X-ray diffractometer. Samples were prepared drop-casting on Si substrates. DFT calculations were performed by using the Gaussian 09 program. The stable ground-state geometries in the gas phase were optimized at the ωB97XD/6-31G*. The analytical Hessians at all stationary points were computed to calculate thermal correction to Gibbs free energy. The empirical dispersion corrections (which were calculated by using the empirical formula by Grimme) were applied.

Device Fabrication and Characterization. Conventional OSCs were fabricated, and the device structures are shown as follows: ITO/V_2O_5/polymer:$PC_{71}BM$/Ca/Al. ITO-coated glass was ultrasonically washed in detergent, deionized water, acetone, and 2-propanol sequentially for 20 min each. Afterward, the cleaned ITO-coated glass was exposed to oxygen plasma to remove organic contaminants and to increase the size of the wetting envelope. The V_2O_5 layer was prepared through spin-coating a vanadium(V) triisopropoxide oxide alcohol solution (2.5% (v/v)) at 4000 rpm on ITO substrates and then was treated under O_2 plasma for 10 min, without the need for hydrolysis with moisture, or annealed. Subsequently, the modified ITO-coated glass was moved to the glovebox. Polymers and $PC_{71}BM$ were dissolved in *o*-DCB. The solution was stirred overnight at room temperature and then heated for 1 h at 100 °C before being spin-coated on V_2O_5 modified ITO-coated glass to form the active layer. The devices were then deposited by Ca (10 nm)/Al (100 nm) as cathode through a shadow mask under high vacuum (~10^{-4} Pa). The thickness of the active layer was controlled by changing the spin speed or solution concentration and was estimated using Veeco Dektak 150 surface profiler. The devices area was 0.1 cm^2 defined by a shadow mask. Current density−voltage (J−V) characteristics of the OSCs were recorded using Keithley 2420 source measurement unit under the illumination of AM 1.5G (100 mW cm^{-2}, Newport solar simulator). Light intensity was calibrated with a standard silicon solar cell. The

DOI: 10.1021/acs.chemmater.7b03025
Chem. Mater. 2017, 29, 9162−9170

external quantum efficiencies (EQEs) of solar cells were analyzed using a certified Newport incident photon conversion efficiency (IPCE) measurement system. Hole mobility was measured using the space charge limited current (SCLC) model with device configuration of ITO/PEDOT:PSS/polymer:$PC_{71}BM$/MoO_3/Ag by taking current−voltage in the range of 0−5 V and fitting the results to a space charge limited form for a hole-only device. In the presence of carrier traps in the active layer, a trap-filled-limit (TFL) region exists between the ohmic and trap-free SCLC regions. The SCLC behavior in the trap-free region can be characterized by using the Mott−Gurney equation,

$$J = \frac{9\varepsilon\mu V^2}{8L^3}$$

where ε is the static dielectric constant of the medium and μ is the carrier mobility, L is the polymer thickness, and V is the voltage drop across the device. $V = V_{app}$-V_{bi}-Vs, where V_{app} is the voltage applied to the device, and V_{bi} is the built-in voltage resulting from the relative work function difference between the two electrodes, V_S is the voltage drop due to contact resistance and series resistance across the electrodes.

■ ASSOCIATED CONTENT

Supporting Information

The Supporting Information is available free of charge on the ACS Publications website at DOI: 10.1021/acs.chemmater.7b03025.

Monomer and polymer synthesis; UV−vis spectra and cyclic voltammetry measurement; DFT calculations and GIWAXS patterns; SCLC results and ^1H and ^{13}CNMR spectra; and the device optimization conditions (PDF)

■ AUTHOR INFORMATION

Corresponding Authors

*(X.Wan) E-mail:wanxb@qibebt.ac.cn.
*(R.Y.) E-mail: yangrq@qibebt.ac.cn.
*(Z.L.) E-mail:Lanzg@qibebt.ac.cn.

ORCID

Xichang Bao: 0000-0001-7325-7550
Renqiang Yang: 0000-0001-6794-7416
Xiaobo Wan: 0000-0001-5740-512X

Author Contributions

All authors have given approval to the final version of the manuscript. M.C., X.B., and Y.L. contributed equally to this work.

Notes

The authors declare no competing financial interest.

■ ACKNOWLEDGMENTS

We thank the National Science Foundation of China (Grant Nos. NSFC51573204, 21402220, 21607164, and 51573205) for financial support of this research. X.B. thanks the Youth Innovation Promotion Association CAS for financial support (Grant No. 2016194). We also thank the Shanghai Synchrotron Radiation Facility for providing beam time on beamline BL16B1.

■ REFERENCES

(1) Bin, H.; Zhang, Z. G.; Gao, L.; Chen, S.; Zhong, L.; Xue, L.; Yang, C.; Li, Y. Non-Fullerene Polymer Solar Cells Based on Alkylthio and Fluorine Substituted 2D-Conjugated Polymers Reach 9.5% Efficiency. *J. Am. Chem. Soc.* **2016**, *138*, 4657−4664.

(2) Hu, H.; Jiang, K.; Yang, G.; Liu, J.; Li, Z.; Lin, H.; Liu, Y.; Zhao, J.; Zhang, J.; Huang, F.; Qu, Y.; Ma, W.; Yan, H. Terthiophene-Based D-A Polymer with an Asymmetric Arrangement of Alkyl Chains That Enables Efficient Polymer Solar Cells. *J. Am. Chem. Soc.* **2015**, *137*, 14149−14157.

(3) Liu, Y.; Zhao, J.; Li, Z.; Mu, C.; Ma, W.; Hu, H.; Jiang, K.; Lin, H.; Ade, H.; Yan, H. Aggregation and morphology control enables multiple cases of high-efficiency polymer solar cells. *Nat. Commun.* **2014**, *5*, 5293.

(4) Ma, W.; Yang, G. F.; Jiang, K.; Carpenter, J. H.; Wu, Y.; Meng, X. Y.; McAfee, T.; Zhao, J. B.; Zhu, C. H.; Wang, C.; Ade, H.; Yan, H. Influence of Processing Parameters and Molecular Weight on the Morphology and Properties of High-Performance PffBT4T-2OD:PC71BM Organic Solar Cells. *Adv. Energy Mater.* **2015**, *5*, 1501400.

(5) Zhao, J.; Li, Y.; Hunt, A.; Zhang, J.; Yao, H.; Li, Z.; Zhang, J.; Huang, F.; Ade, H.; Yan, H. A Difluorobenzoxadiazole Building Block for Efficient Polymer Solar Cells. *Adv. Mater.* **2016**, *28*, 1868−1873.

(6) Yao, H.; Cui, Y.; Yu, R.; Gao, B.; Zhang, H.; Hou, J. Design, Synthesis, and Photovoltaic Characterization of a Small Molecular Acceptor with an Ultra-Narrow Band Gap. *Angew. Chem., Int. Ed.* **2017**, *56*, 3045−3049.

(7) Dou, C. D.; Long, X. J.; Ding, Z. C.; Xie, Z. Y.; Liu, J.; Wang, L. X. An Electron-Deficient Building Block Based on the B → N Unit: An Electron Acceptor for All-Polymer Solar Cells. *Angew. Chem., Int. Ed.* **2016**, *55*, 1436−1440.

(8) Liu, S. J.; Kan, Z. P.; Thomas, S.; Cruciani, F.; Bredas, J. L.; Beaujuge, P. M. Thieno[3,4-c]pyrrole-4,6-dione-3,4-difluorothiophene Polymer Acceptors for Efficient All-Polymer Bulk Heterojunction Solar Cells. *Angew. Chem., Int. Ed.* **2016**, *55*, 12996−13000.

(9) Liang, Y.; Feng, D.; Wu, Y.; Tsai, S. T.; Li, G.; Ray, C.; Yu, L. Highly Efficient Solar Cell Polymers Developed via Fine-Tuning of Structural and Electronic Properties. *J. Am. Chem. Soc.* **2009**, *131*, 7792−7799.

(10) Fan, Q. P.; Su, W. Y.; Guo, X.; Guo, B.; Li, W. B.; Zhang, Y. D.; Wang, K.; Zhang, M. J.; Li, Y. F. A New Polythiophene Derivative for High Efficiency Polymer Solar Cells with PCE over 9%. *Adv. Energy Mater.* **2016**, *6*, 1600430.

(11) He, D.; Geng, X. J.; Ding, L. M. The effect of fluorination on the photovoltaic performance of the D-A copolymers containing naphtho-[2,3-c] thiophene-4,9-dione and bithiophene moieties. *Polym. Chem.* **2016**, *7*, 4993−4997.

(12) Jo, J. W.; Jung, J. W.; Wang, H. W.; Kim, P.; Russell, T. P.; Jo, W. H. Fluorination of Polythiophene Derivatives for High Performance Organic Photovoltaics. *Chem. Mater.* **2014**, *26*, 4214−4220.

(13) Kawashima, K.; Fukuhara, T.; Suda, Y.; Suzuki, Y.; Koganezawa, T.; Yoshida, H.; Ohkita, H.; Osaka, I.; Takimiya, K. Implication of Fluorine Atom on Electronic Properties, Ordering Structures, and Photovoltaic Performance in Naphthobisthiadiazole-Based Semiconducting Polymers. *J. Am. Chem. Soc.* **2016**, *138*, 10265−10275.

(14) Wang, J.; Bao, X.; Ding, D.; Qiu, M.; Du, Z.; Wang, J.; Liu, J.; Sun, M.; Yang, R. A fluorine-induced high-performance narrow bandgap polymer based on thiadiazolo[3,4-c]pyridine for photovoltaic applications. *J. Mater. Chem. A* **2016**, *4*, 11729−11737.

(15) Carsten, B.; Szarko, J. M.; Son, H. J.; Wang, W.; Lu, L. Y.; He, F.; Rolczynski, B. S.; Lou, S. J.; Chen, L. X.; Yu, L. P. Examining the Effect of the Dipole Moment on Charge Separation in Donor-Acceptor Polymers for Organic Photovoltaic Applications. *J. Am. Chem. Soc.* **2011**, *133*, 20468−20475.

(16) Guo, S.; Ning, J.; Körstgens, V.; Yao, Y.; Herzig, E. M.; Roth, S. V.; Müller-Buschbaum, P. The Effect of Fluorination in Manipulating the Nanomorphology in PTB7:$PC_{71}BM$ Bulk Heterojunction Systems. *Adv. Energy Mater.* **2015**, *5*, 1401315.

(17) Son, H. J.; Wang, W.; Xu, T.; Liang, Y. Y.; Wu, Y. E.; Li, G.; Yu, L. P. Synthesis of Fluorinated Polythienothiophene-co-benzodithiophenes and Effect of Fluorination on the Photovoltaic Properties. *J. Am. Chem. Soc.* **2011**, *133*, 1885−1894.

(18) Duan, C.; Furlan, A.; van Franeker, J. J.; Willems, R. E. M.; Wienk, M. M.; Janssen, R. A. J. Wide-Bandgap Benzodithiophene-

DOI: 10.1021/acs.chemmater.7b03025
Chem. Mater. 2017, 29, 9162−9170

Benzothiadiazole Copolymers for Highly Efficient Multijunction Polymer Solar Cells. *Adv. Mater.* **2015**, *27*, 4461−4468.
(19) Jo, J. W.; Jung, J. W.; Jung, E. H.; Ahn, H.; Shin, T. J.; Jo, W. H. Fluorination on both D and A units in D−A type conjugated copolymers based on difluorobithiophene and benzothiadiazole for highly efficient polymer solar cells. *Energy Environ. Sci.* **2015**, *8*, 2427−2434.
(20) Jung, J. W.; Liu, F.; Russell, T. P.; Jo, W. H. Medium Bandgap Conjugated Polymer for High Performance Polymer Solar Cells Exceeding 9% Power Conversion Efficiency. *Adv. Mater.* **2015**, *27*, 7462−7468.
(21) Liu, Y.; Zhao, W.; Wu, Y.; Zhang, J.; Li, G.; Li, W.; Ma, W.; Hou, J.; Bo, Z. Enhancing the power conversion efficiency of polymer solar cells to 9.26% by a synergistic effect of fluoro and carboxylate substitution. *J. Mater. Chem. A* **2016**, *4*, 8097−8104.
(22) Shi, S. B.; Liao, Q. G.; Tang, Y. M.; Guo, H.; Zhou, X.; Wang, Y. L.; Yang, T. B.; Liang, Y. Y.; Cheng, X.; Liu, F.; Guo, X. G. Head-to-Head Linkage Containing Bithiophene-Based Polymeric Semiconductors for Highly Efficient Polymer Solar Cells. *Adv. Mater.* **2016**, *28*, 9969−9977.
(23) Wang, J. L.; Yin, Q. R.; Miao, J. S.; Wu, Z.; Chang, Z. F.; Cao, Y.; Zhang, R. B.; Wang, J. Y.; Wu, H. B.; Cao, Y. Rational Design of Small Molecular Donor for Solution-Processed Organic Photovoltaics with 8.1% Efficiency and High Fill Factor via Multiple Fluorine Substituents and Thiophene Bridge. *Adv. Funct. Mater.* **2015**, *25*, 3514−3523.
(24) Wang, M.; Cai, D. D.; Yin, Z. G.; Chen, S. C.; Du, C. F.; Zheng, Q. D. Asymmetric-Indenothiophene-Based Copolymers for Bulk Heterojunction Solar Cells with 9.14% Efficiency. *Adv. Mater.* **2016**, *28*, 3359−3365.
(25) Gao, L.; Zhang, Z. G.; Xue, L. W.; Min, J.; Zhang, J. Q.; Wei, Z. X.; Li, Y. F. All-Polymer Solar Cells Based on Absorption-Complementary Polymer Donor and Acceptor with High Power Conversion Efficiency of 8.27%. *Adv. Mater.* **2016**, *28*, 1884−1890.
(26) Li, W. T.; Albrecht, S.; Yang, L. Q.; Roland, S.; Tumbleston, J. R.; McAfee, T.; Yan, L.; Kelly, M. A.; Ade, H.; Neher, D.; You, W. Mobility-Controlled Performance of Thick Solar Cells Based on Fluorinated Copolymers. *J. Am. Chem. Soc.* **2014**, *136*, 15566−15576.
(27) Price, S. C.; Stuart, A. C.; Yang, L.; Zhou, H.; You, W. Fluorine Substituted Conjugated Polymer of Medium Band Gap Yields 7% Efficiency in Polymer−Fullerene Solar Cells. *J. Am. Chem. Soc.* **2011**, *133*, 4625−4631.
(28) Zhou, C.; Zhang, G.; Zhong, C.; Jia, X.; Luo, P.; Xu, R.; Gao, K.; Jiang, X.; Liu, F.; Russell, T. P.; Huang, F.; Cao, Y. Toward High Efficiency Polymer Solar Cells: Influence of Local Chemical Environment and Morphology. *Adv. Energy Mater.* **2017**, *7*, 1601081.
(29) Do, K.; Saleem, Q.; Ravva, M. K.; Cruciani, F.; Kan, Z.; Wolf, J.; Hansen, M. R.; Beaujuge, P. M.; Brédas, J. L. Impact of Fluorine Substituents on π-Conjugated Polymer Main-Chain Conformations, Packing, and Electronic Couplings. *Adv. Mater.* **2016**, *28*, 8197−8205.
(30) Chen, Z. H.; Brown, J.; Drees, M.; Seger, M.; Hu, Y.; Xia, Y.; Boudinet, D.; McCray, M.; Delferro, M.; Marks, T. J.; Liao, C. Y.; Ko, C. W.; Chang, Y. M.; Facchetti, A. Benzo[d][1,2,3]thiadiazole (isoBT): Synthesis, Structural Analysis, and Implementation in Semiconducting Polymers. *Chem. Mater.* **2016**, *28*, 6390−6400.
(31) Wang, M.; Ford, M.; Phan, H.; Coughlin, J.; Nguyen, T. Q.; Bazan, G. C. Fluorine substitution influence on benzo[2,1,3]-thiadiazole based polymers for field-effect transistor applications. *Chem. Commun.* **2016**, *52*, 3207−3210.
(32) Oh, J.; Kranthiraja, K.; Lee, C.; Gunasekar, K.; Kim, S.; Ma, B.; Kim, B. J.; Jin, S. H. Side-Chain Fluorination: An Effective Approach to Achieving High-Performance All-Polymer Solar Cells with Efficiency Exceeding 7%. *Adv. Mater.* **2016**, *28*, 10016−10023.
(33) Wang, N.; Chen, W.; Shen, W.; Duan, L.; Qiu, M.; Wang, J.; Yang, C.; Du, Z.; Yang, R. Novel donor−acceptor polymers containing o-fluoro-p-alkoxyphenyl-substituted benzo[1,2-b:4,5-b′]dithiophene units for polymer solar cells with power conversion efficiency exceeding 9%. *J. Mater. Chem. A* **2016**, *4*, 10212−10222.
(34) Shin, J.; Kim, M.; Lee, J.; Kim, H. G.; Hwang, H.; Cho, K. Positional effects of fluorination in conjugated side chains on photovoltaic properties of donor−acceptor copolymers. *Chem. Commun.* **2017**, *53*, 1176−1179.
(35) Lei, T.; Xia, X.; Wang, J. Y.; Liu, C. J.; Pei, J. Conformation Locked" Strong Electron-Deficient Poly(p-Phenylene Vinylene) Derivatives for Ambient-Stable n-Type Field-Effect Transistors: Synthesis, Properties, and Effects of Fluorine Substitution Position. *J. Am. Chem. Soc.* **2014**, *136*, 2135−2141.
(36) Cai, M.; Bao, X. C.; Wang, X.; Zhang, H. R.; Qiu, M.; Yang, R. Q.; Yang, C. M.; Wan, X. B. From Isoindigo to Dibenzonaphthyridinedione: A Building Block for Wide-Bandgap Conjugated Polymers with High Power Conversion Efficiency. *Chem. Mater.* **2016**, *28*, 6196−6206.
(37) Lei, T.; Cao, Y.; Zhou, X.; Peng, Y.; Bian, J.; Pei, J. Systematic Investigation of Isoindigo-Based Polymeric Field-Effect Transistors: Design Strategy and Impact of Polymer Symmetry and Backbone Curvature. *Chem. Mater.* **2012**, *24*, 1762−1770.
(38) Yao, H.; Ye, L.; Hou, J.; Jang, B.; Han, G.; Cui, Y.; Su, G. M.; Wang, C.; Gao, B.; Yu, R.; Zhang, H.; Yi, Y.; Woo, H. Y.; Ade, H.; Hou, J. Achieving Highly Efficient Nonfullerene Organic Solar Cells with Improved Intermolecular Interaction and Open-Circuit Voltage. *Adv. Mater.* **2017**, *29*, 1700254.
(39) Drees, M.; Hoppe, H.; Winder, C.; Neugebauer, H.; Sariciftci, N. S.; Schwinger, W.; Schäffler, F.; Topf, C.; Scharber, M. C.; Zhu, Z.; Gaudiana, R. Stabilization of the nanomorphology of polymer−fullerene "bulk heterojunction" blends using a novel polymerizable fullerene derivative. *J. Mater. Chem.* **2005**, *15*, 5158−5163.
(40) Heeger, A. J. 25th Anniversary Article: Bulk Heterojunction Solar Cells: Understanding the Mechanism of Operation. *Adv. Mater.* **2014**, *26*, 10−28.
(41) Shaw, P. E.; Ruseckas, A.; Samuel, I. D. W. Exciton diffusion measurements in poly(3-hexylthiophene). *Adv. Mater.* **2008**, *20*, 3516−3520.
(42) Ma, W.; Yang, G.; Jiang, K.; Carpenter, J. H.; Wu, Y.; Meng, X.; McAfee, T.; Zhao, J.; Zhu, C.; Wang, C.; Ade, H.; Yan, H. Influence of Processing Parameters and Molecular Weight on the Morphology and Properties of High-Performance PffBT4T-2OD: $PC_{71}BM$ Organic Solar Cells. *Adv. Energy Mater.* **2015**, *5*, 1501400.
(43) Cao, X. X.; Li, M. G.; Liu, J. G.; Wang, H. Y.; Zhou, K.; Han, Y. C. Control over fibril width via different solubility additives for diketopyrrolopyrrole-based photovoltaic devices. *Org. Electron.* **2015**, *24*, 280−287.
(44) van Franeker, J. J.; Heintges, G. H. L.; Schaefer, C.; Portale, G.; Li, W.; Wienk, M. M.; van der Schoot, P.; Janssen, R. A. J. Polymer Solar Cells: Solubility Controls Fiber Network Formation. *J. Am. Chem. Soc.* **2015**, *137*, 11783−11794.

DOI: 10.1021/acs.chemmater.7b03025
Chem. Mater. 2017, 29, 9162−9170